19

Sliding Mode Control Applied to a Novel Linear Axis Actuated by Pneumatic Muscles

Dominik Schindele and Harald Aschemann
Chair of Mechatronics, University of Rostock
18059 Rostock, Germany

1. Introduction

Pneumatic muscles are innovative tensile actuators consisting of a fiber-reinforced vulcanised rubber tubing with appropriate connectors at both ends. The working principle is based on a rhombical fibre structure that leads to a muscle contraction in longitudinal direction when the pneumatic muscle is filled with compressed air. This contraction can be used for actuation purposes. Pneumatic muscles are low cost actuators and offer several further advantages in comparison to classical pneumatic cylinders: significantly less weight, no stick-slip effects, insensitivity to dirty working environment, and a higher force-to-weight ratio. A major advantage of pneumatic drives as compared to electrical drives is their capability of providing large maximum forces for a longer period of time. In this case electrical drives are in risk of overheating and may result in increasing errors due to thermal expansion. For these reasons, different researchers have investigated pneumatic muscles as actuators for several applications, e.g. a planar elbow manipulator in Lilly & Yang (2005), a 2-DOF serial manipulator in Van-Damme et al. (2007) or a parallel manipulator in Zhu et al. (2008).
Pneumatic muscles are characterised by dominant nonlinearities, namely the force and volume characteristics. Hence, these nonlinearities have to be considered by suitable control approaches such as sliding mode control. In this contribution the sliding mode technique is applied to a novel linear drive actuated by four pneumatic muscles. This pneumatic linear drive allows for maximum velocities of approximately 1.3 m/s in a workspace of approximately 1 m. In Aschemann & Hofer (2004) and Aschemann et al. (2006) the authors presented the implementation of a trajectory control for a carriage with a pair of pneumatic muscles arranged at opposite sides of a carriage. Unfortunately, this direct actuation by pneumatic muscles suffers from two main drawbacks: On the one hand, the maximum velocity of the carriage is limited to approx. 0.3 m/s, on the other hand the workspace is constrained to the maximum contraction length of the pneumatic muscles, in the given case to approx. 0.25 m. To increase the available workspace as well as the maximum carriage velocity, a new test-rig has been built up. At this test-rig, a rocker transmits the drive force of the pneumatic muscles to the carriage, see Aschemann & Schindele (2008) or Schindele & Aschemann (2010). One disadvantage of this setup is the required height, necessary for the kinematics considered there. To reduce the overall size of the drive mechanism, now, the muscle force is transmitted to the carriage by a pulley tackle consisting of a wire rope and several deflection pulleys, see Fig. 1. The mentioned components are installed such that the required muscle force as well as the maximum workspace and velocity of the carriage are

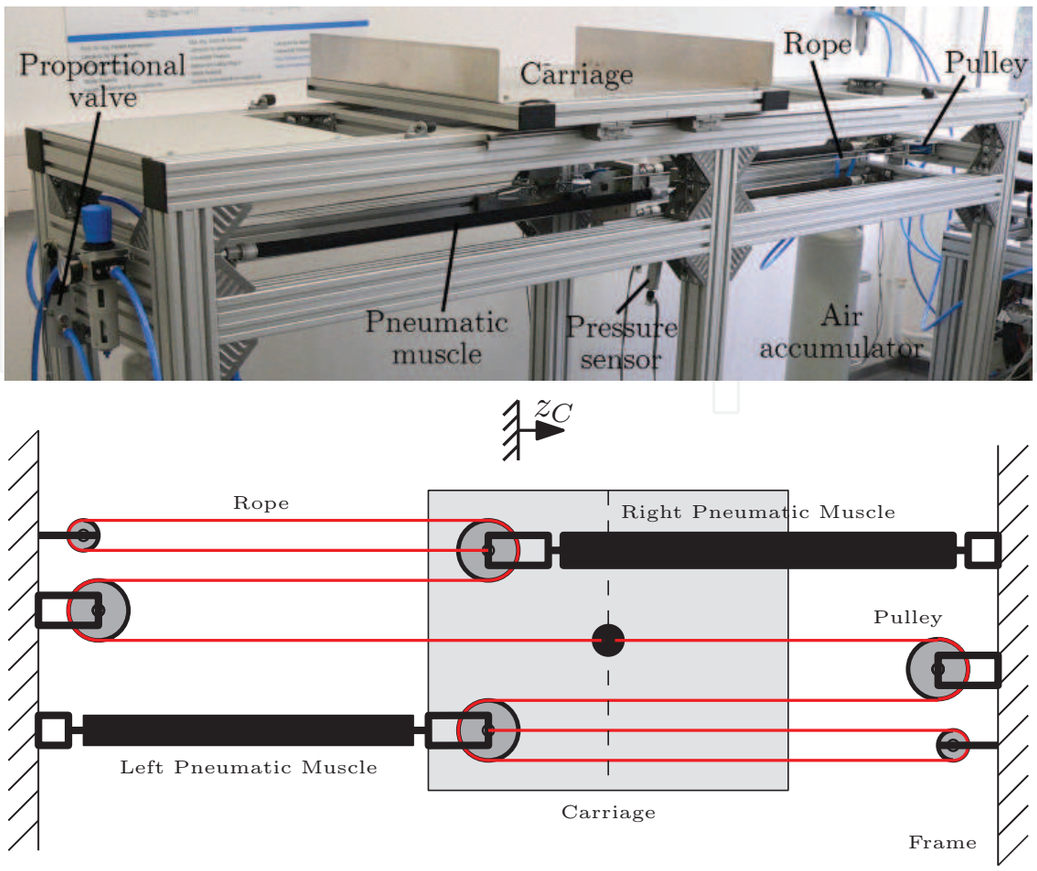

Figure 1. Experimental setup.

increased by a factor of three, in comparison to a directly driven configuration. For actuation of the carriage, four pneumatic muscles are employed, whereas two muscles are used for each direction of tension, respectively. The mass flow rate of compressed air in and accordingly out of each pneumatic muscle is controlled by means of two separate proportional valves. One proportional valve is employed for the two left pneumatic muscles and the other proportional valve is utilised for the two right pneumatic muscles. Pressure declines in the case of large mass flow rates are avoided by using an air accumulator for each valve.

In the paper, first, a control-oriented model of the pneumatically driven high-speed linear axis is derived in section 2 as the basis of control design. At this, polynomial descriptions are utilised to describe the nonlinear characteristics of the pneumatic muscle, i.e., the muscle volume and the muscle force as functions of both contraction length and internal muscle pressure. Second, in sections 3 and 4, sliding mode control techniques are employed to design a nonlinear cascade control. For this purpose the differential flatness-property of the system is exploited. The inner control loops involve a fast pressure control for each muscle, respectively. The outer control loop achieves a decoupling of the carriage position and the mean muscle pressure as controlled variables and provides the reference pressures for the inner pressure control loops. As an alternative to the standard sliding mode technique, additionally, a second-order sliding mode controller and a proxy-based sliding mode controller has been designed for the outer control loop. Proxy-based sliding mode control is a modification of sliding mode control as well as an extension of PID-control, see Kikuuwe & Fujimoto

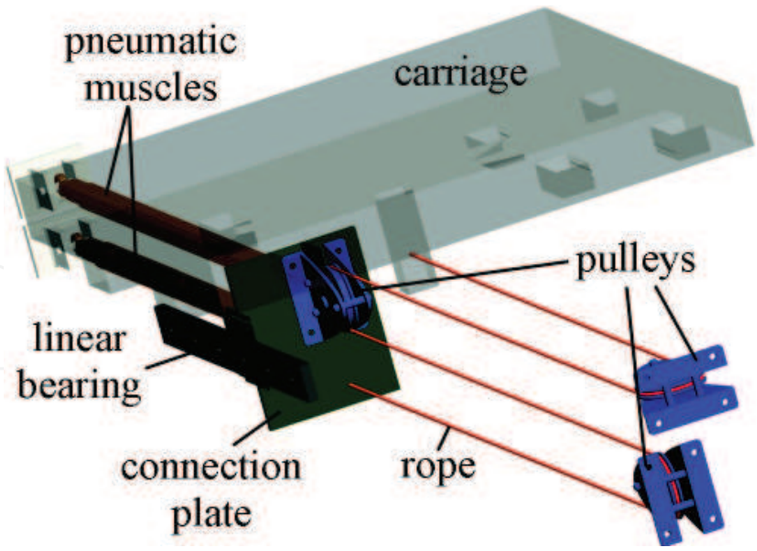

Figure 2. Drawing of the left pulley tackle.

(2006), Van-Damme et al. (2007). The basic idea is to introduce a virtual carriage, called proxy, which is controlled using sliding mode techniques, whereas the proxy is connected to the real carriage by a PID-type coupling force. The goal is to achieve precise tracking during normal operation and smooth, overdamped recovery in the presence of large position errors, which leads to an inherent safety property. In sections 5 and 6, nonlinear friction and remaining model uncertainties in the equations of motion are considered by a feedforward friction compensation module, based on the LuGre model in combination with a nonlinear reduced-order disturbance observer. Finally, in section 8, the proposed control strategy has been implemented at the test rig of the Chair of Mechatronics, University of Rostock. Thereby, desired trajectories for the carriage position can be tracked with high accuracy.

2. System modelling

The modelling of the pneumatically driven high-speed linear axis involves the mechanical subsystem and the pneumatic subsystem, which are coupled by the tension forces of the pneumatic muscles.

2.1 Modelling of the mechanical subsystem

The mechanical model of the high-speed linear axis consists of the carriage and two pulley tackles, at which one pulley tackle transmits the tension force of two pneumatic muscles to the carriage in each case. In this way two pneumatic muscles as well as one pulley tackle is employed for each moving direction of the carriage, see Fig. 2. For modelling the mechanical subsystem is divided into the following elements (Fig. 1 and Fig. 2): a lumped mass for the carriage (mass m_C), the two connection plates, which are also modelled as lumped masses (mass m_{MFi}, $i = \{l,r\}$) and the six pulleys (mass moment of inertia J_{ij}, $i = \{l,r\}$, $j = \{1,2,3\}$). The motion of the linear axis is completely described by the generalised coordinate $z_C(t)$, which denotes the carriage position. The equation of motion directly follows from Lagrange's equations in form of a second-order differential equation

$$m \cdot \ddot{z}_C = \frac{a_M}{k} \left(F_{Mr} - F_{Ml} \right) - F_U \, , \tag{1}$$

with the reduced mass

$$m = \frac{1}{k^2}\left(k^2 \cdot m_C + m_{MFl} + m_{MFr} + \sum_{j=1}^{3} J_{lj}\left(\frac{j}{r}\right)^2 + \sum_{j=1}^{3} J_{rj}\left(\frac{j}{r}\right)^2\right). \tag{2}$$

The parameter $k = 3$ denotes the number of pulleys (radius r) employed for each pulley tackle, and the parameter $a_M = 2$ stands for the two muscles, used for actuation in the left or right direction, respectively. All remaining model uncertainties are taken into account by the disturbance force F_U. On the one hand, these uncertainties stem from approximation errors concerning the static muscle force characteristics and non-modelled viscoelastic effects of the vulcanised rubber material. On the other hand, time-varying damping and friction acting on the carriage, the connection plates and the pulleys depend in a complex manner on lots of influence factors and cannot be accurately represented by a simple friction model.

2.2 Modelling of the pneumatic subsystem

Under the assumption, that the dynamic behaviour of the internal muscle pressure is identically for the two left and right muscles, for modelling and control of the pneumatic subsystem only one muscle for each drive direction is considered. The larger force obtained by utilising two muscles for each pulley tackle is regarded by the factor α_M in equation (1). A mass flow $\dot{m}_{Mi}$, $i = \{l, r\}$ into the pneumatic muscle leads to an increase in internal pressure p_{Mi}, and a contraction $\Delta\ell_{Mi}$ of the muscle in longitudinal direction due to specially arranged fibers. The maximum contraction length $\Delta\ell_{M,max}$ is given by 25% of the uncontracted length. This contraction effect can be exploited to generate forces. The force F_{Mi} and the volume V_{Mi} of a pneumatic muscle depend nonlinear on the according internal pressure p_{Mi} and the contraction length $\Delta\ell_{Mi}$. Given the length of the uncontracted muscle ℓ_M, the contraction length of a pneumatic muscle is related to the carriage position by the following equations

$$\Delta\ell_{Ml} = \ell_M - \frac{1}{k} z_C \,, \tag{3}$$

$$\Delta\ell_{Mr} = \ell_M + \frac{1}{k} z_C \,. \tag{4}$$

The dynamics of the internal muscle pressure follows directly from a mass flow balance in combination with the energy equation for the compressed air in the muscle. As the internal muscle pressure is limited by a maximum value of $p_{Mi,max} = 7$ bar, the ideal gas equation represents an accurate description of the thermodynamic behaviour of the air in muscle $i = \{l, r\}$ (Smith et al. (1996))

$$\frac{p_{Mi}}{\rho_{Mi}} = R_L \cdot T_{Mi} \,. \tag{5}$$

Here, the density ρ_{Mi}, the gas constant of air R_L and the thermodynamic temperature T_{Mi} are introduced. The thermodynamic process is modelled as a polytropic change of state (Smith et al. (1996))

$$\frac{p_{Mi}}{\rho_{Mi}^n} = const. \tag{6}$$

with $n = 1.26$ as identified polytropic exponent. The polytropic exponent is in between $n = 1$ for an isothermal process, and $n = \kappa$ for an isentropic process. Thus, the relationship between the time derivative of the pressure and the time derivative of the density is given by

$$\dot{p}_{Mi} = n \cdot R_L \cdot T_{Mi} \cdot \dot{\rho}_{Mi} \,. \tag{7}$$

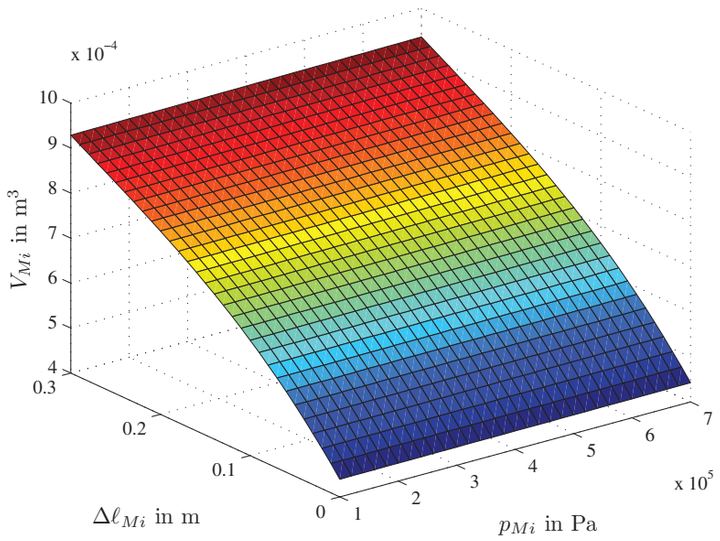

Figure 3. Identified volume characteristic of the pneumatic muscle.

The mass flow balance for the pneumatic muscle is governed by

$$\dot{\rho}_{Mi} \cdot V_{Mi} = \dot{m}_{Mi} - \rho_{Mi} \cdot \dot{V}_{Mi} \tag{8}$$

The identified volume characteristic (Fig. 3) of the pneumatic muscle can be described by a polynomial function of both contraction length $\Delta\ell_{Mi}$ and the muscle pressure p_{Mi}

$$V_{Mi}\left(\Delta\ell_{Mi}, p_{Mi}\right) = \sum_{j=0}^{3} a_j \cdot \Delta\ell_{Mi}^{j} \cdot \sum_{k=0}^{1} b_k \cdot p_{Mi}^{k}. \tag{9}$$

By inserting (7) and (9), the pressure dynamics (8) for the muscle i results in

$$\begin{aligned} \dot{p}_{Mi} &= \frac{n}{V_{Mi} + n \cdot \frac{\partial V_{Mi}}{\partial p_{Mi}} \cdot p_{Mi}} \left[u_{Mi} - \frac{\partial V_{Mi}}{\partial \Delta\ell_{Mi}} \cdot \frac{\mathrm{d}\Delta\ell_{Mi}}{\mathrm{d}z_C} \cdot p_{Mi} \cdot \dot{z}_C \right] \\ &= k_{ui}\left(\Delta\ell_{Mi}, p_{Mi}\right) u_{Mi} - k_{pi}\left(\Delta\ell_{Mi}, \Delta\dot{\ell}_{Mi}, p_{Mi}\right) p_{Mi}, \end{aligned} \tag{10}$$

where $u_{Mi} = R_L \cdot T_{Mi} \cdot \dot{m}_{Mi}$ denotes the input variable. The internal temperature T_{Mi} can be approximated with good accuracy by the constant temperature T_{amb} of the ambiance. In this way, temperature measurements are avoided, and the implementational effort is significantly reduced.

The force characteristic $F_{Mi}\left(p_{Mi}, \Delta\ell_{Mi}\right)$ of a pneumatic muscle states the resulting tension force for given internal pressure p_{Mi} as well as given contraction length $\Delta\ell_{Mi}$ and represents the connection of the mechanical and the pneumatic system part. The nonlinear force characteristic (Fig. 4) has been identified by static measurements and, then, approximated by the following polynomial description

$$F_{Mi}(p_{Mi}, \Delta\ell_{Mi}) = \begin{cases} \bar{F}_{Mi}(p_{Mi}, \Delta\ell_{Mi}), & \bar{F}_{Mi} > 0 \\ 0 & , \text{ else} \end{cases}, \tag{11}$$

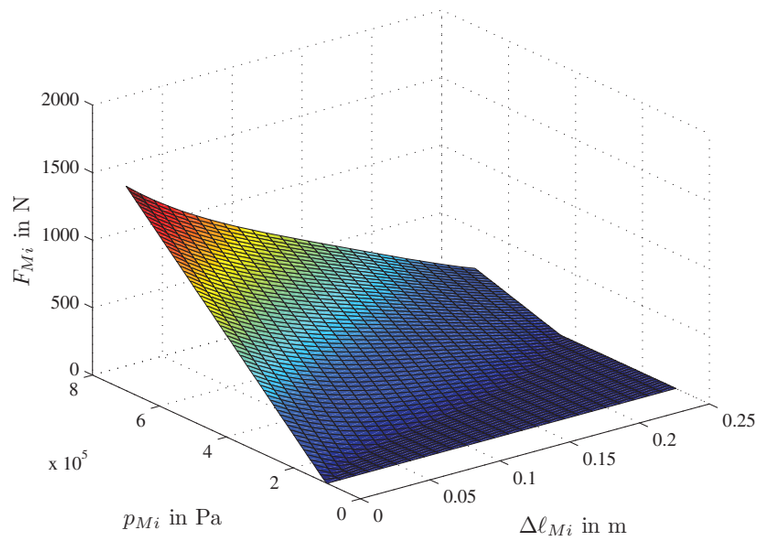

Figure 4. Identified force characteristic of the pneumatic muscle.

with

$$\bar{F}_{Mi}(p_{Mi}, \Delta l_{Mi}) = \underbrace{\sum_{m=0}^{3} \left(a_m \cdot \Delta\ell_{Mi}^m\right) p_{Mi}}_{f_{1i}} - \underbrace{\sum_{n=0}^{4} \left(b_n \cdot \Delta\ell_{Mi}^n\right)}_{f_{2i}} . \tag{12}$$

3. Control of the carriage position

The different sliding mode controllers for the carriage position are designed by exploiting the differential flatness property of the system under consideration (Fliess et al. (1995), Sira-Ramirez & Llanes-Santiago (2000)). For the mechanical system the carriage position z_C and the mean muscle pressure $p_M = 0.5\,(p_{Ml} + p_{Mr})$ are chosen as flat output candidates. The trajectory control of the mean pressure allows for increasing stiffness concerning disturbance forces acting on the carriage (Bindel et al. (1999)). As the inner controls have been assigned a high bandwidth, these underlying controlled muscle pressures can be considered as ideal control inputs of the outer control

$$\boldsymbol{u} = \begin{bmatrix} u_l \\ u_r \end{bmatrix} = \begin{bmatrix} p_{Ml} \\ p_{Mr} \end{bmatrix} . \tag{13}$$

Subsequent differentiation of the first flat output candidate until one of the control inputs appears leads to

$$y_1 = z_C, \tag{14a}$$

$$\dot{y}_1 = \dot{z}_C, \tag{14b}$$

$$\ddot{y}_1 = \frac{a_M}{k \cdot m}\left(F_{Mr} - F_{Ml}\right) - \frac{1}{m} F_U = \ddot{z}_C\left(z_C, \dot{z}_C, p_{Ml}, p_{Mr}, F_U\right), \tag{14c}$$

whereas the second variable directly depends on the control inputs

$$y_2 = p_M = 0.5\,(p_{Ml} + p_{Mr}) . \tag{15}$$

The disturbance force F_U is estimated by a disturbance observer and used for disturbance compensation. Due to the differential flatness of the system, the inverse dynamics can be obtained by solving the equations (14) and (15) for the input variables

$$\boldsymbol{u} = \frac{1}{a_M\left(f_{1l}+f_{1r}\right)}\begin{bmatrix} a_M f_{2l} - a_M f_{2r} - km\ddot{z}_C - kF_U + 2a_M p_M f_{1r} \\ a_M f_{2r} - a_M f_{2l} + km\ddot{z}_C + kF_U + 2a_M p_M f_{1l} \end{bmatrix} . \tag{16}$$

3.1 Sliding mode control

Now, the tracking error $e_z = z_{Cd} - z_C$ can be stabilised by sliding mode control. For this purpose, the following sliding surface s_z is defined for the outer control loop in the form

$$s_z = \dot{z}_{Cd} - \dot{z}_C + \alpha\left(z_{Cd} - z_C\right) . \tag{17}$$

At this, the coefficient α must be chosen positive in order to obtain a Hurwitz-polynomial. The convergence to the sliding surfaces in face of model uncertainty can be achieved by specifying a discontinuous signum-function

$$\dot{s}_z = -W_z \cdot sign(s_z), \;\; W_z > 0. \tag{18}$$

With a properly chosen positive coefficient W_z dominating the corresponding model uncertainties, the sliding surface $s_z = 0$ is reached in finite time depending on the initial conditions. This leads to the stabilising control law for each crank angle

$$v_z = \ddot{q}_{id} + \alpha \cdot (\dot{z}_{Cd} - \dot{z}_C) + W_z \cdot sign(s_z). \tag{19}$$

Here, the carriage position z_C, the carriage velocity $\dot{z}_C$, the desired trajectory for the carriage position z_{Cd} and their first two time derivatives have to be provided. For the second stabilising control input v_p, the desired trajectory for the mean pressure p_{Md} is directly utilised in a feedforward manner, i.e., $v_p = p_{Md}$. Inserting these new defined inputs into (16), the inverse dynamics becomes

$$\boldsymbol{u} = \frac{1}{a_M\left(f_{1l}+f_{1r}\right)}\begin{bmatrix} a_M f_{2l} - a_M f_{2r} - kmv_z - kF_U + 2a_M v_p f_{1r} \\ a_M f_{2r} - a_M f_{2l} + kmv_z + kF_U + 2a_M v_p f_{1l} \end{bmatrix} . \tag{20}$$

Having once reached the sliding surfaces, the final sliding mode is maintained during trajectory tracking provided that the tracking error $e_z = z_{Cd} - z_C$ is governed by an asymptotically stable first-order error dynamics

$$\dot{e}_z + \alpha \cdot e_z = 0. \tag{21}$$

Then, a globally asymptotically stable tracking of desired trajectories for the carriage position is guaranteed leading to

$$\lim_{t\to\infty} e_z(t) = 0. \tag{22}$$

For reduction of high frequency chattering the switching function $sign(s_z)$ in (19) can be replaced by the smooth function $\tanh\left(\frac{s_z}{\epsilon}\right)$, $\epsilon > 0$

$$v_z = \ddot{z}_{Cd} + \alpha \cdot (\dot{z}_{Cd} - \dot{z}_C) + W_z \cdot \tanh\left(\frac{s_z}{\epsilon}\right). \tag{23}$$

This regularisation, however, implicates a non-ideal sliding mode within a resulting boundary layer determined by the parameter ϵ in the switching function.

3.2 Higher-order sliding mode control

An alternative method to reduce high frequency chattering effects is to employ higher-order sliding mode techniques for control design, Levant (2008). For this approach the control derivative is considered as a new control input. Containing an integrator in the dynamic feedback law, real discontinuities in the control input are avoided at higher-order sliding mode. In this contribution a quasi-continuous second-order sliding mode controller as proposed in Levant (2005) is utilised. Then the tracking error is stabilised by the following control law

$$v_z = \alpha \frac{\dot{s}_z + \beta \left|s_z\right|^{\frac{1}{2}} sign\left(s_z\right)}{\left|\dot{s}_z\right| + \beta \left|s\right|^{\frac{1}{2}}} \,. \tag{24}$$

In Pukdeboon et al. (2010) a slightly modified version of this controller is introduced. For a reduction of the chattering phenomena, a small positive scalar ν is added to the denominator of (24). Then the smoothed control law is given by

$$v_z = \alpha \frac{\dot{s}_z + \beta \left|s_z\right|^{\frac{1}{2}} sign\left(s_z\right)}{\left|\dot{s}_z\right| + \beta \left|s\right|^{\frac{1}{2}} + \nu} \,. \tag{25}$$

For further reduction of the chattering phenomena, similar to the first-order sliding mode control law (23) the discontinuous function $sign\left(s_z\right)$ in (25) can be replaced by the smooth function $\tanh\left(\frac{s_z}{\epsilon}\right)$, $\epsilon > 0$. Again, the new control input v_z has to be inserted in the inverse dynamics (16), at which the second control input v_p remains the same.

3.3 Proxy-based sliding mode control

Proxy-based sliding mode control is a modification of sliding mode control as well as an extension of PID-control, see Kikuuwe & Fujimoto (2006), Van-Damme et al. (2007). The basic idea is to introduce a virtual carriage, called proxy, which is controlled using sliding mode techniques, whereas the proxy is connected to the real carriage by a PID-type coupling force, see Fig. 5. The goal of proxy-based sliding mode is to achieve precise tracking during normal operation and smooth, overdamped recovery in case of large position errors. The sliding mode control law for the virtual carriage results from equation (19) with z_S denoting the carriage position of the proxy

$$v_a = \ddot{z}_{Cd} + \alpha \cdot \left(\dot{z}_{Cd} - \dot{z}_S\right) + W_z \cdot tanh\left(\frac{\dot{z}_{Cd} - \dot{z}_s + \alpha\left(z_{Cd} - z_S\right)}{\epsilon}\right). \tag{26}$$

The PID-type virtual coupling between the proxy and the real carriage is given by

$$v_c = K_I \int \left(z_S - z_C\right) \mathrm{dt} + K_P\left(z_S - z_C\right) + K_D\left(\dot{z}_s - \dot{z}_C\right). \tag{27}$$

Assuming a proxy with vanishing mass, the condition $v_a = v_c$ holds. By introducing the new variable a as integrated difference between the real and the virtual carriage position $a = \int \left(z_S - z_C\right) \mathrm{dt}$, the virtual coupling (27) and the stabilising proxy-based sliding mode control law (26) result in (Kikuuwe & Fujimoto (2006))

$$v_c = K_I a + K_P \dot{a} + K_D \ddot{a} \,, \tag{28}$$

$$v_a = \ddot{z}_{Cd} + \alpha \dot{e}_z - \alpha \ddot{a} + W_z tanh\left(\frac{\dot{e}_z + \alpha e_z - \alpha \dot{a} - \ddot{a}}{\epsilon}\right) \,. \tag{29}$$

The implementation of the control law is shown in the right part of Fig. 5.

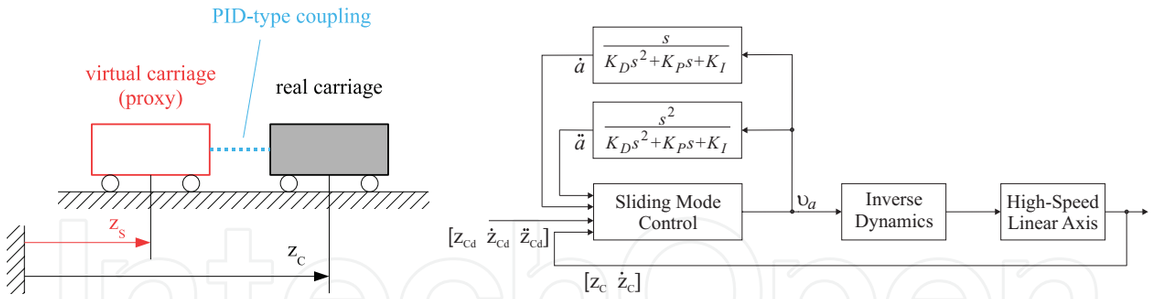

Figure 5. Coupling between virtual and real carriage (left). Implementation of the proxy-based sliding mode control (right).

4. Control of internal muscle pressure

The internal pressures of the pneumatic muscles are controlled separately with high accuracy in fast underlying control loops. The pneumatic subsystem represents a differentially flat system with the internal muscle pressure as flat output, see Aschemann & Schindele (2008). Hence, equation (10) can be solved for the input variable

$$u_{Mi} = \frac{1}{k_{ui}\left(\Delta\ell_{Mi}, p_{Mi}\right)}\left[\dot{p}_{Mi} + k_{pi}\left(\Delta\ell_{Mi}, \Delta\dot{\ell}_{Mi}, p_{Mi}\right) p_{Mi}\right] . \tag{30}$$

The contraction length $\Delta\ell_{Mi}$ as well as its time derivative $\Delta\dot{\ell}_{Mi}$ can be considered as scheduling parameters in a gain-scheduled adaptation of k_{ui} and k_{pi}. With the internal pressure as flat output, its first time derivative $\dot{p}_{Mi} = v_i$ is introduced as new control input. The error dynamics of each muscle pressure $p_{Mi}, i = \{l, r\}$, can be asymptotically stabilised by the following control law

$$v_i = \dot{p}_{Mid} + a_i \cdot \left(p_{Mid} - p_{Mi}\right) , \tag{31}$$

where the constant a_i is determined by pole placement. By introducing the definition $e_i = p_{Mid} - p_{Mi}$ for the control error w.r.t. the internal muscle pressure, the corresponding error dynamics is governed by the following first order differential equation

$$\dot{e}_i + a_i \cdot \dot{e}_i = 0 . \tag{32}$$

5. Feedforward friction compensation

The main part of the friction is considered by a dynamical friction model in a feedforward manner. For this purpose, the LuGre friction model, introduced by de Wit et al. (1995), is employed. This friction model is capable of describing the Stribeck effect, hysteresis, stick-slip limit cycling, presliding displacement as well as rising static friction

$$\dot{z} = \dot{z}_{Cd} - \frac{|\dot{z}_{Cd}|}{g\left(\dot{z}_{Cd}\right)} z , \tag{33}$$

$$F_{Fr} = \sigma_0 z + \sigma_1 \dot{z} + \sigma_2 \dot{z}_{Cd} , \tag{34}$$

where the function $g\left(\dot{z}_{Cd}\right)$ is given by

$$g\left(\dot{z}_{Cd}\right) = F_C + \left(F_S - F_C\right) e^{-\left(\frac{\dot{z}_{Cd}}{v_S}\right)^2} . \tag{35}$$

Here, the internal state variable z describes the deflection of the contact surfaces. The model parameters are given by the static friction F_S, the Coulomb friction F_C and the Stribeck velocity v_S. The parameter σ_0 is the stiffness coefficient, σ_1 the damping coefficient and σ_2 the viscous friction coefficient. All parameters have been identified using nonlinear least square techniques.

6. Reduced nonlinear disturbance observer

Disturbance behaviour and tracking accuracy in view of model uncertainties can be significantly improved by introducing a compensating control action provided by a nonlinear reduced-order disturbance observer as described in Friedland (1996). The observer design is based on the equation of motion. The key idea for the observer design is to extend the state equation with integrators as disturbance models

$$\begin{aligned} \dot{\mathbf{y}} &= \mathbf{f}\left(\mathbf{y}, F_U, \mathbf{u}\right) \,, \\ \dot{F}_U &= 0 \,, \end{aligned} \tag{36}$$

where $\mathbf{y} = \left[\, \mathbf{q} \;\; \dot{\mathbf{q}} \,\right]^T$ denotes the measurable state vector. The estimated disturbance force $\hat{F}_U$ is obtained from $\hat{F}_U = \mathbf{h}^T\mathbf{y} + z$ with the chosen observer gain vector $\mathbf{h}^T$.

$$\mathbf{h}^T = \left[\, h_1 \;\; h_1 \,\right] \,. \tag{37}$$

The state equation for z is given by

$$\dot{z} = \Phi\left(\mathbf{y}, \hat{F}_U, \mathbf{u}\right) \,. \tag{38}$$

The observer gain vector $\mathbf{h}$ and the nonlinear function Φ have to be chosen such that the steady-state observer error $e = F_U - \hat{F}_U$ converges to zero. Thus, the function Φ can be determined as follows

$$\dot{e} = 0 = \dot{F}_U - h^T\mathbf{f}\left(\mathbf{y}, \hat{F}_U, \mathbf{u}\right) - \Phi\left(\mathbf{y}, F_U, \mathbf{u}\right) \,. \tag{39}$$

In view of $\dot{F}_U = 0$, equation (39) yields

$$\Phi\left(\mathbf{y}, F_U, \mathbf{u}\right) = -\mathbf{h}^T\mathbf{f}\left(\mathbf{y}, \hat{F}_U\mathbf{u}\right) \,. \tag{40}$$

The linearised error dynamics $\dot{e}$ has to be made asymptotically stable. Accordingly, all eigenvalues of the Jacobian

$$\mathbf{J}_e = \frac{\partial\Phi\left(\mathbf{y}, F_U, \mathbf{u}\right)}{\partial F_U} \tag{41}$$

must be located in the left complex half-plane. This can be achieved by proper choice of the observer gain h_1. The stability of the closed-loop control system has been investigated by thorough simulations.

7. Control implementation

For the implementation at the test rig the control structure as depicted in Fig. 6 has been used. Fast underlying pressure control loops achieve an accurate tracking behaviour for the desired pressures stemming from the outer control loop. The nonlinear valve characteristic (VC) has been identified by measurements, see Aschemann & Schindele (2008), and is compensated by

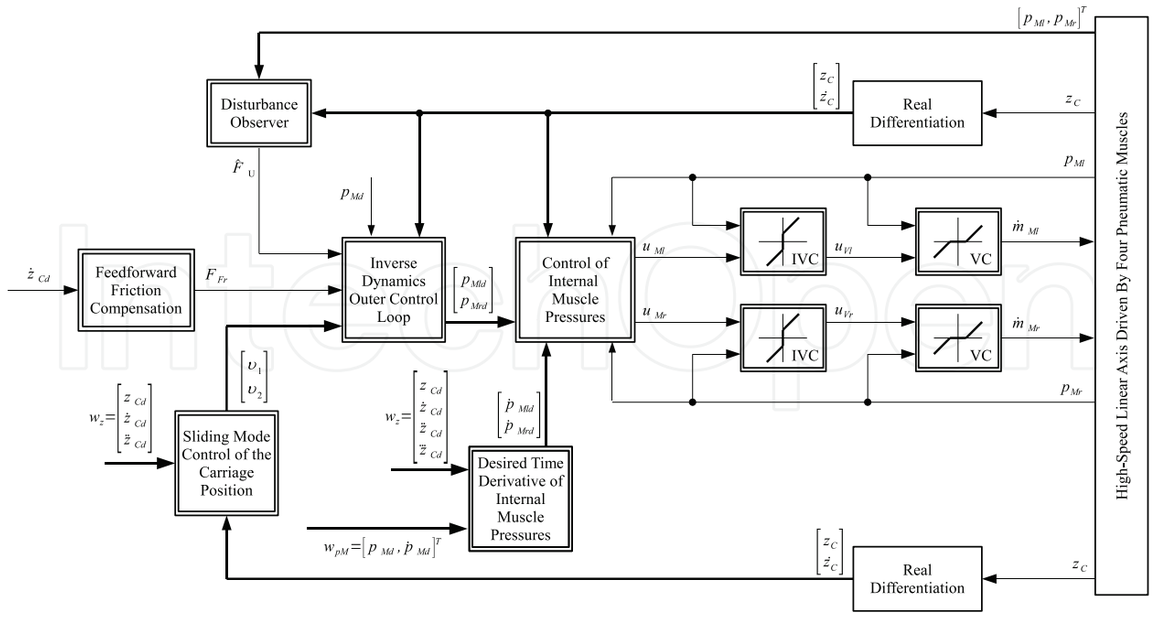

Figure 6. Implementation of the cascaded control structure.

its approximated inverse valve characteristic (IVC) in each input channel. For each pulley tackle one pneumatic muscle is equipped with a piezo-resistive pressure sensor mounted at the connection flange that connects the muscle with the connection plate. The carriage position z_C is obtained by a linear incremental encoder providing high resolution. The carriage velocity $\dot{z}_C$ is derived from the carriage position z_C by means of real differentiation using a DT_1-System with the corresponding transfer function $G_{DT1}(s) = \frac{s}{T_1 s+1}$. The desired value for the time derivative of the internal muscle pressure can be obtained either by real differentiation of the corresponding control input p_{Mi} in (16) or by model-based calculation using only desired values, i.e.

$$\dot{p}_{Mid} = \dot{p}_{Mid}\left(z_{Cd}, \dot{z}_{Cd}, \ddot{z}_{Cd}, \dddot{z}_{Cd}, p_{Md}, \dot{p}_{Md}, \hat{F}_U, \dot{\hat{F}}_U\right). \tag{42}$$

The corresponding desired trajectories are obtained from a trajectory planning module that provides synchronous time optimal trajectories according to given kinematic and dynamic constraints. It becomes obvious that a continuous time derivative $\dot{p}_{Mid}$ requires a three times continuously differentiable desired carriage trajectory. In (42) the time derivative of $\hat{F}_U$ is needed. Considering equation (38) and the first time derivatives of the system states, the value of $\dot{\hat{F}}_U$ can be obtained as follows

$$\dot{\hat{F}}_U = \mathbf{h}^T \dot{\mathbf{y}} + \dot{z}. \tag{43}$$

8. Experimental results

Both tracking performance and steady-state accuracy w.r.t. the carriage position z_C have been investigated by experiments at the test rig of the Chair of Mechatronics, University of Rostock. It is equipped with four pneumatic muscles DMSP-20 from FESTO AG. The control algorithm has been implemented on a dSpace real time system. For the experiments the trajectory shown in Fig. 7 have been used. Here the desired carriage position varies in an interval between

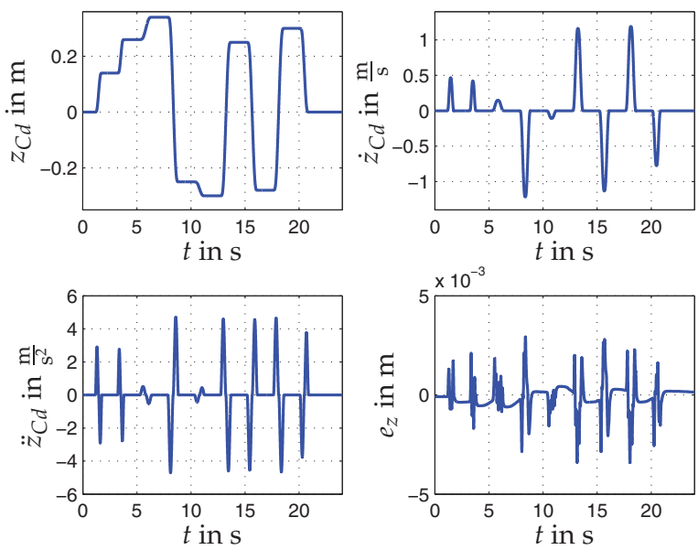

Figure 7. Desired values for the carriage position, velocity, and acceleration. Corresponding control error $e_z = z_{Cd} - z_C$ for standard sliding mode control.

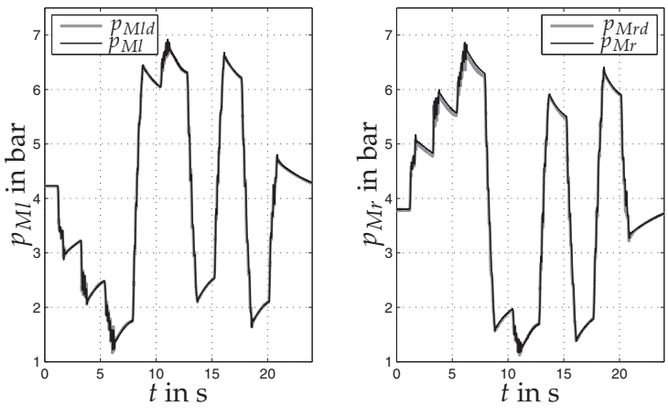

Figure 8. Comparison of desired and actual values for the left and right muscle pressure.

-0.35 m and 0.35 m. The maximum velocities are approximately 1.3 m/s and the maximum accelerations are about 5 m/s^2. The resulting tracking errors for the carriage $e_z = z_{Cd} - z_C$ are shown in the right lower part of Fig. 7. As for the carriage position, the maximum tracking error during the acceleration and deceleration intervals is approximately 3.5 mm. The maximum steady-state error is approximately 0.6 mm. Fig. 8 shows the corresponding desired and actual values of the internal muscle pressure. Obviously, the underlying fast control loops achieve a precise tracking of the desired values, which stem from the outer decoupling control loop. Due to a time-optimal trajectory planning using desired ansatzfunctions with limited jerk as described in Aschemann & Hofer (2005), the admissible range of the internal muscle pressure is not exceeded. In Fig. 9 the different control approaches, introduced in this contribution, are compared concerning the control error e_z. The higher-order sliding mode (HOSM) control approach results in a slightly larger maximum tracking error than

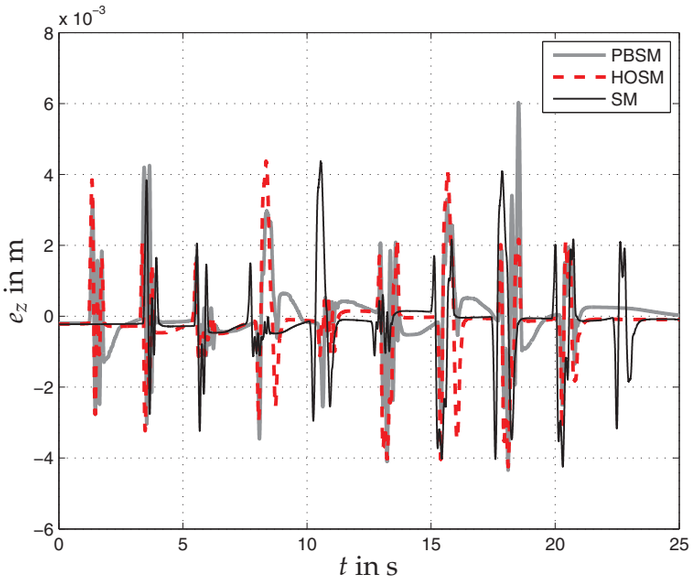

Figure 9. Comparison of different control approaches concerning the corresponding control errror e_z: Proxy-based sliding mode control (PBSM), Higher-order sliding mode control (HOSM) and standard sliding mode control (SM).

with the standard sliding mode technique (SM). Nevertheless, the steady-state accuracy of the HOSM approach is superior to the other approaches. As the chattering phenomena is reduced by HOSM control the parameter ϵ in equation (25) can be chosen very small, so that the hyperbolic tangent function is very close to the ideal switching-function. The parameter ϵ in (23) have to be chosen about 100 times larger as compared to the value in HOSM, to avoid the high-frequency chattering, which is critical for the proportional valves and results in a reduced lifetime of the valves. The largest tracking errors occur with proxy-based sliding mode (PBSM) control, which represents a PID-controller at normal operation. The benefits of the PBSM control are its high robustness and its slow and safe recovery from unexpected disturbances and abnormal events, which leads to an inherent safety property. In Fig. 10 the impact of the feedforward friction compensation and the nonlinear reduced disturbance observer is demonstrated. Here the tracking errors of SM control with feedforward friction compensation (f.f.c.) and disturbance observer (d.o.), SM control only with f.f.c and SM control without f.f.c. and d.o. are depicted. As can be seen the tracking errors can be significantly reduced by employing the proposed disturbance compensation strategy. The sum of the feedforward friction force F_{Fr} and the disturbance force estimated by the disturbance observer $\hat{F}_U$ is depicted in Fig. 11. The robustness of the proposed solution is shown by a unmodelled additional mass of 25 kg, which represents almost the double of the nominal value. In the corresponding force, the increase due to the higher inertial forces becomes obvious. The corresponding tracking errors are shown in Fig. 12. All three control approaches show similar results. Whereas the steady-state errors remain almost unchanged, the maximum tracking errors are now approximately 8 mm due to the inertia forces during the acceleration and deceleration phases. The closed-loop stability is not affected by this parametric uncertainty.

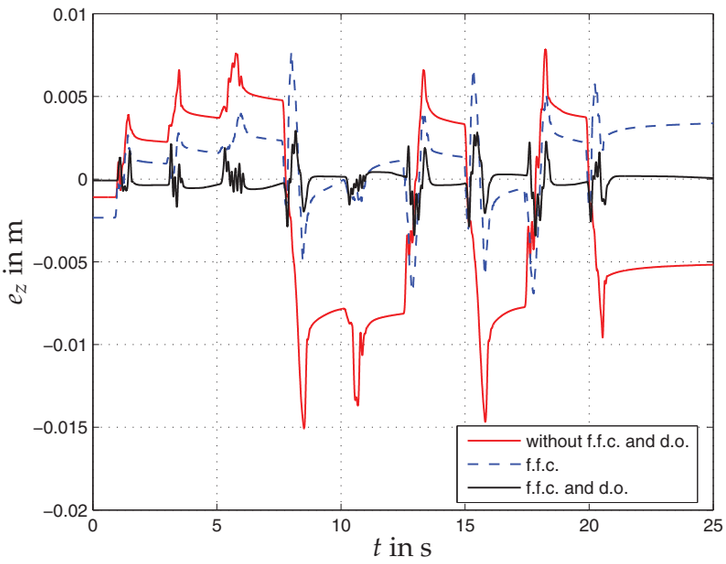

Figure 10. Tracking errors of SM control without disturbance compensation, SM control with feedforward friction compensation (f.f.c.) and SM control with f.f.c. and disturbance observer (d.o.).

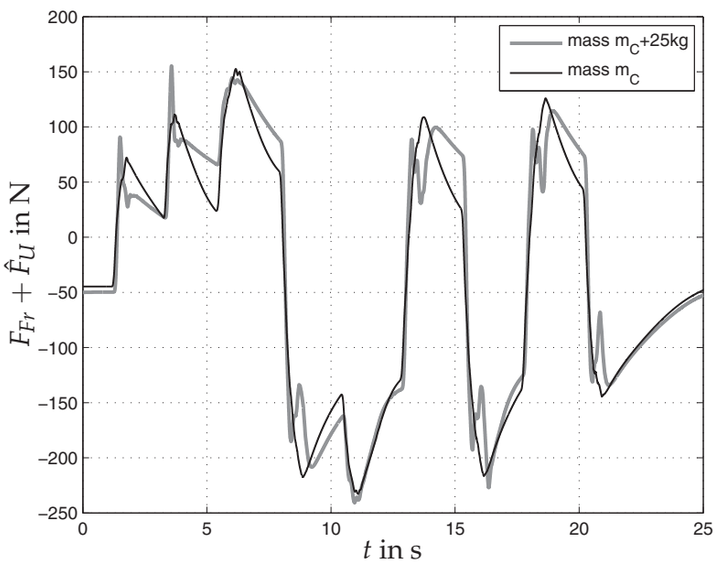

Figure 11. Estimated disturbance force with and without additional mass of 25 kg.

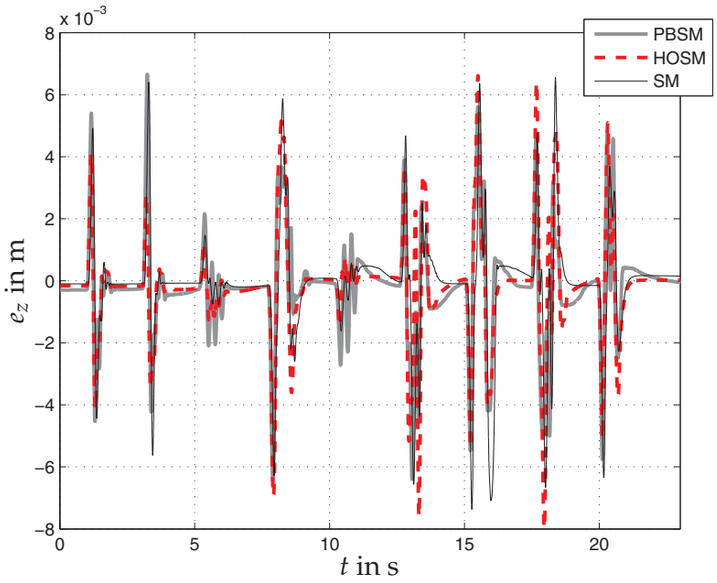

Figure 12. Tracking errors with an additional mass of 25 kg.

9. Conclusions

In this paper, a nonlinear cascaded trajectory control was presented for a new linear axis driven by pneumatic muscles that offers a significant increase in both workspace and maximum velocity as compared to a directly actuated solution. Furthermore, the proposed setup requires a relativ small overall size in comparison to a drive concept with an rocker as in Aschemann & Schindele (2008). The modelling of this mechatronic system leads to nonlinear system equations of fourth order containing identified polynomial descriptions of the main nonlinearities of the pneumatic subsystem: the characteristic of the pneumatic valve and the characteristics of the pneumatic muscle. The inner control loops of the cascade involve a decentralised control of the internal muscle pressures with high bandwidth. For the outer control loop different sliding mode control approaches have been investigated leading to a decoupling of the carriage position and the mean pressure as controlled variables. Thereby, critical high frequency chattering can be avoided either by a regularisation of the switching function or by using a second-order sliding mode controller. Model uncertainties in the muscle force characteristic as well as nonlinear friction are directly taken into account by a compensation scheme consisting of a feedforward friction compensation and a nonlinear reduced disturbance observer. Experimental results emphasise the excellent closed-loop performance with maximum position errors of approximately 4 mm. The robustness of the proposed control is shown by measurements with an almost doubled carriage mass.

10. References

Aschemann, H. & Hofer, E. (2004). Flatness-based trajectory control of a pneumatically driven carriage with uncertainties, *Proceedings of NOLCOS 2004, Stuttgart, Germany* pp. 239–244.

Aschemann, H. & Hofer, E. (2005). Flatness-based trajectory planning and control of a parallel robot actuated by pneumatic muscles, *CD-Proceedings of ECCOMAS Thematic Conf. Multibody Dyn., Madrid, Spain* .

Aschemann, H. & Schindele, D. (2008). Sliding-mode control of a high-speed linear axis driven by pneumatic muscle actuators, *IEEE Trans. Ind. Electronics* 55(11): 3855–3864.

Aschemann, H., Schindele, D. & Hofer, E. (2006). Nonlinear optimal control of a mechatronic system with pneumatic muscle actuators, *CD-Proceedings of MMAR 2006, Miedzyzdroje, Poland* .

Bindel, R., Nitsche, R., Rothfuß, R. & Zeitz, M. (1999). Flatness based control of two valve hydraulic joint actuator of a large manipulator, *CD-Proceedings of ECC 1999, Karlsruhe, Germany* .

de Wit, C. C., Olsson, H., Âström, K. & Lischinsky, P. (1995). A new model for control of systems with friction, *IEEE Transactions on Automatic Control* 40(3): 419–425.

Fliess, M., Levine, J., Martin, P. & Rouchon, P. (1995). Flatness and defect of nonlinear systems: Introductory theory and examples, *Int. J. Control* 61: 1327–1361.

Friedland, B. (1996). *Advanced Control System Design*, Prentice-Hall.

Kikuuwe, R. & Fujimoto, H. (2006). Proxy-based sliding mode control for accurate and safe position control, *IEEE Trans. on Industr. Electr.* 53(5): 25–30.

Levant, A. (2005). Quasi-continuous high-order sliding-mode controllers, *IEEE Transactions on Automatic Control* 50(11): 1812–1816.

Levant, A. (2008). Homogeneous high-order sliding modes, *Proceedings of the 17th IFAC World Congress, Seoul, Korea* pp. 3799–3810.

Lilly, J. & Yang, L. (2005). Sliding mode control tracking for pneumatic muscle actuators in opposing pair configuration, *IEEE Trans. on Contr. Syst. Techn.* 13(4): 550–558.

Pukdeboon, C., Zinober, A. S. I. & Thein, M.-W. L. (2010). Quasi-continuous higher order sliding-mode controllers for spacecraft-attitude-tracking maneuvers, *IEEE Transactions on Industrial Electronics* 57(4): 1436–1444.

Schindele, D. & Aschemann, H. (2010). Norm-optimal iterative learning control for a high-speed linear axis with pneumatic muscles, *Proc. of NOLCOS 2010, Bologna, Italy*. to be published.

Sira-Ramirez, H. & Llanes-Santiago, O. (2000). Sliding mode control of nonlinear mechanical vibrations, *J. of Dyn. Systems, Meas. and Control* 122(12): 674–678.

Smith, J., Ness, H. V. & Abott, M. M. (1996). *Introduction to Chemical Engineering Thermodynamics*, McGraw-Hill, New York.

Van-Damme, M., Vanderborght, R., Ham, R. V., Verrelst, B., Daerden, F. & Lefeber, D. (2007). Proxy-based sliding-mode control of a manipulator actuated by pleated pneumatic artificial muscles, *Proc. IEEE Int. Conf. on Robotics and Automation, Rome, Italy* pp. 4355–4360.

Zhu, X., Tao, G., Yao, B. & Cao, J. (2008). Adaptive robust posture control of a parallel manipulator driven by pneumatic muscles, *Automatica* 44(9): 2248–2257.

Sliding Mode Control

Edited by Prof. Andrzej Bartoszewicz

ISBN 978-953-307-162-6
Hard cover, 544 pages
Publisher InTech
Published online 11, April, 2011
Published in print edition April, 2011

The main objective of this monograph is to present a broad range of well worked out, recent application studies as well as theoretical contributions in the field of sliding mode control system analysis and design. The contributions presented here include new theoretical developments as well as successful applications of variable structure controllers primarily in the field of power electronics, electric drives and motion steering systems. They enrich the current state of the art, and motivate and encourage new ideas and solutions in the sliding mode control area.

InTech Europe
University Campus STeP Ri
Slavka Krautzeka 83/A
51000 Rijeka, Croatia
Phone: +385 (51) 770 447
Fax: +385 (51) 686 166
www.intechopen.com

InTech China
Unit 405, Office Block, Hotel Equatorial Shanghai
No.65, Yan An Road (West), Shanghai, 200040, China
中国上海市延安西路65号上海国际贵都大饭店办公楼405单元
Phone: +86-21-62489820
Fax: +86-21-62489821

IntechOpen